doi:10.1038/nature11007

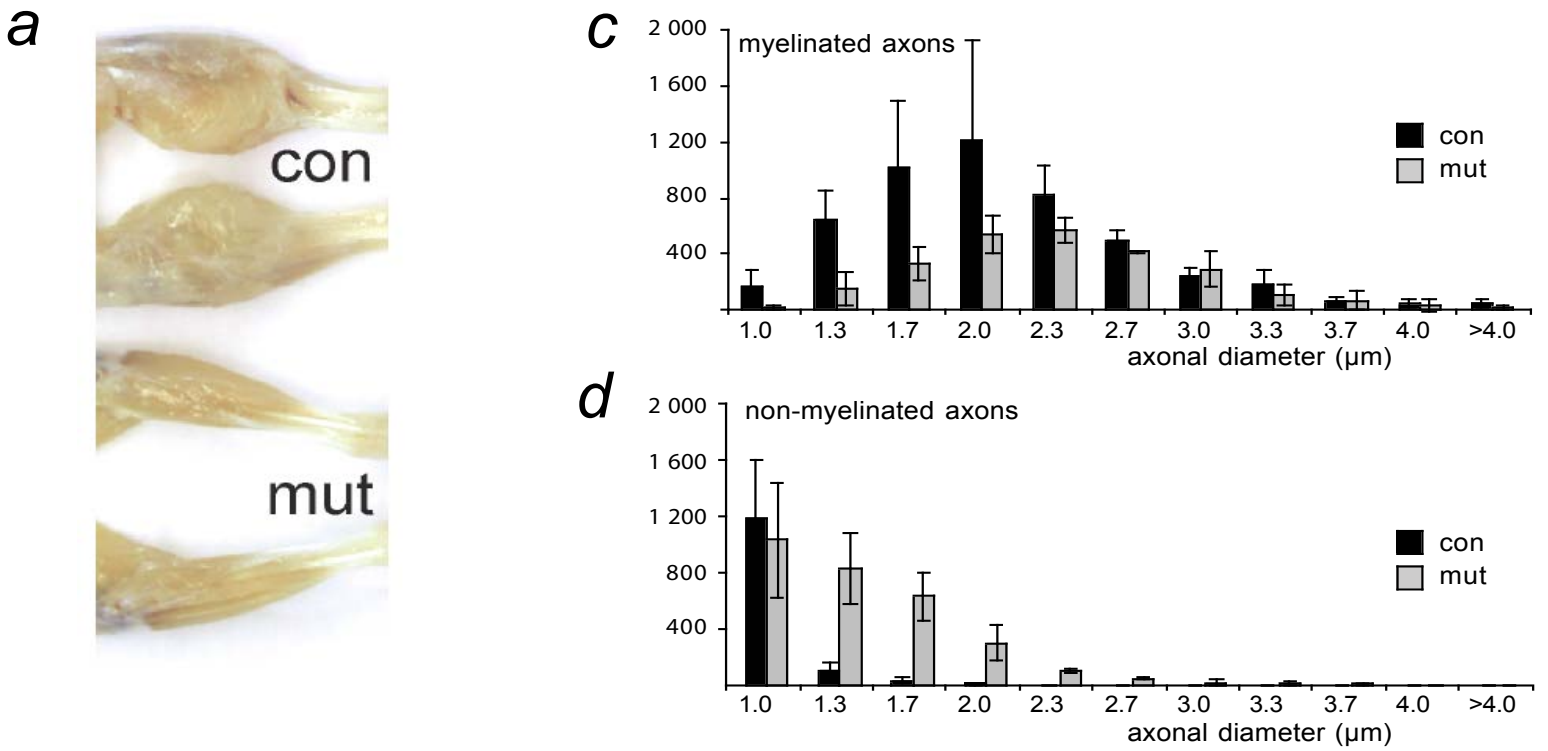

Suppl. Figure 1:

Peripheral neuropathy in *Cnp1^{Cre}*Cox10$^{flox/flox}$* mice

(a) Mutant animals exhibit severe muscle atrophy, as illustrated for dissected calves of control (con) and mutant (mut) mice at age 9 months.

(b) Reduced amplitudes of compound muscle action potentials, triggered by distal stimulation of the sciatic nerve (n=5).

(c, d) Size distribution of myelinated (c) and non-myelinated (d) axons in control mice (con) and mutant mice (mut) at age P21 reveals severe dysmyelination. Axons smaller than 1 µm were excluded from the graph for clarity. Bins are labeled with reference to the upper border. All numbers ± s.d.

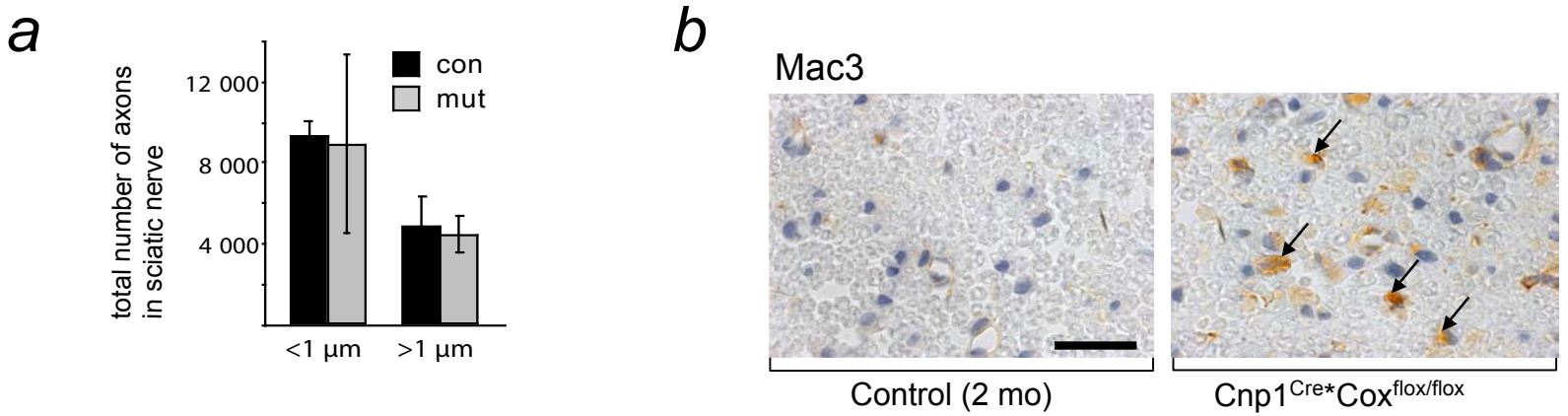

Suppl. Figure 2:

Early neuropathology of peripheral nerves
(a) The total number of axons (±s.d.) in the sciatic nerve is unchanged (age P21).
(b) At age 2 months, numerous Mac3-positive macrophages (arrows) have invaded the mutant sciatic nerve (right), but are rare in controls (left). Scale bar, 20 µm
(c) Electron micrograph of a peripheral axon, myelinated by a *Cox10* mutant Schwann cell that harbors enlarged mitochondria (arrowheads) compared to those in the axon (arrow). Myelin is physically intact. High-pressure frozen sciatic nerves (age P27). Scale bar, 0.5 µm.

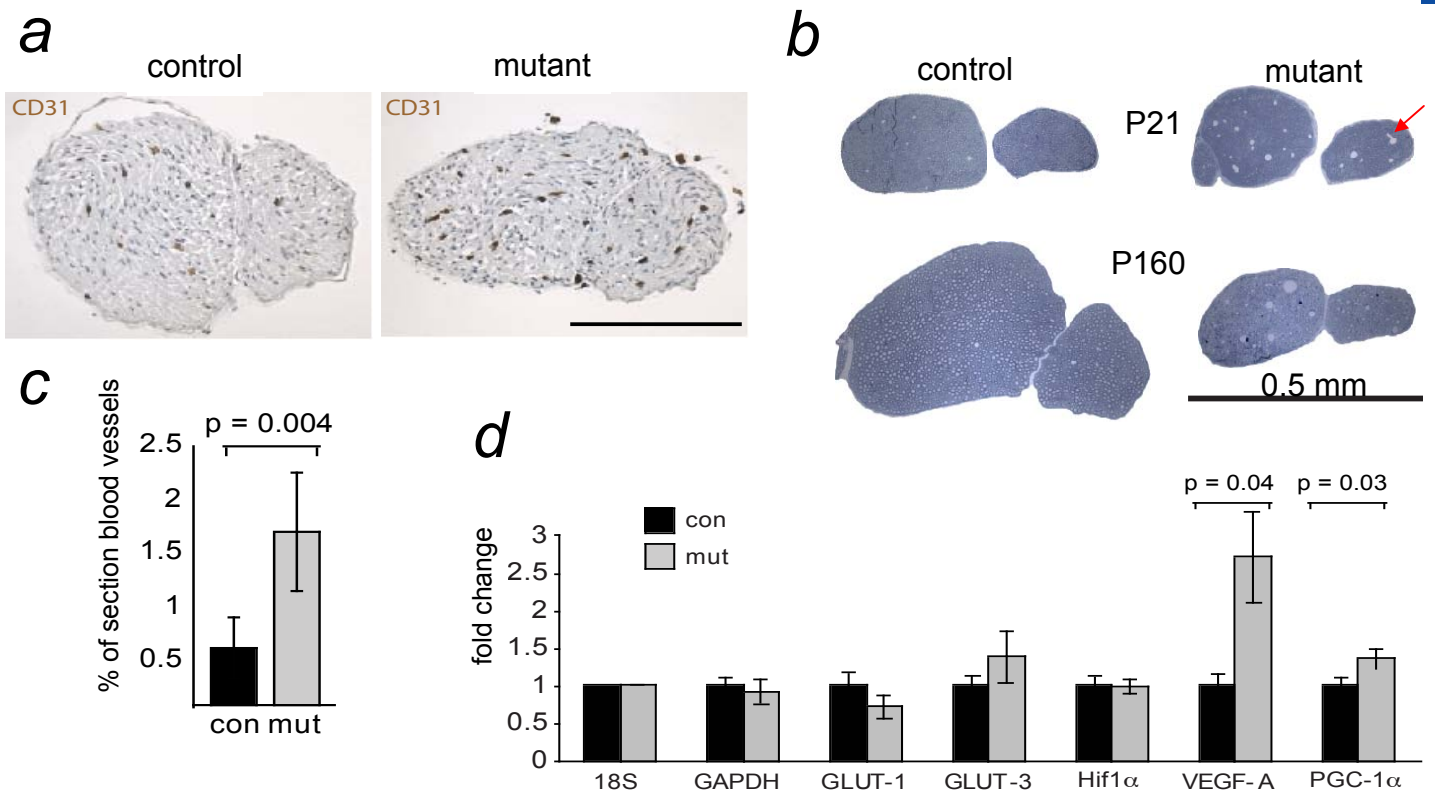

Suppl. Figure 3:

Hypervascularization of peripheral nerves in *Cnp1^{Cre}*Cox10$^{flox/flox}$* mice

(a) Cryosections of sciatic nerves from mutant mice and controls, age P21, were stained for the endothelial marker CD31 (dark brown) to reveal blood vessels. Scale bar, 0.2 mm.

(b) Semithin sections of sciatic nerves from control and mutant mice at early (P21) and late stages (P160), revealing the lack of radial growth (neuropathy) with abnormally enlarged blood vessels (red arrow).

(c) Quantification of endoneurial blood vessels in semi-thin sections of sciatic nerve, demonstrating hypervascularization in mutant mice compared to controls already at age P21 (n=5 per genotype; mean ±s.d.; p-value by one-tailed Student's t-test, assuming unequal variance).

(d) Elevated level of VEGF mRNA in mutant nerves. Quantitative PCRs were performed for glyceraldehydes-3-phosphate dehydrogenase (GAPDH), glucose transporter type 1 (GLUT-1), glucose transporter type3 (GLUT-3), hypoxia-inducible factor 1 alpha (Hif-1α), vascular endothelial factor - A (VEGF-A), and peroxisome-proliferator-activated receptor-gamma coactivator-1 alpha (PGC-1alpha). For mutant (mut) and controls (con), all values were normalized to 18S ribosomal RNA (18S). (n = 4 animals per genotype; mean±s.e.m.; p-values by one-tailed Student's t-test, assuming unequal variance).

doi:10.1038/nature11007

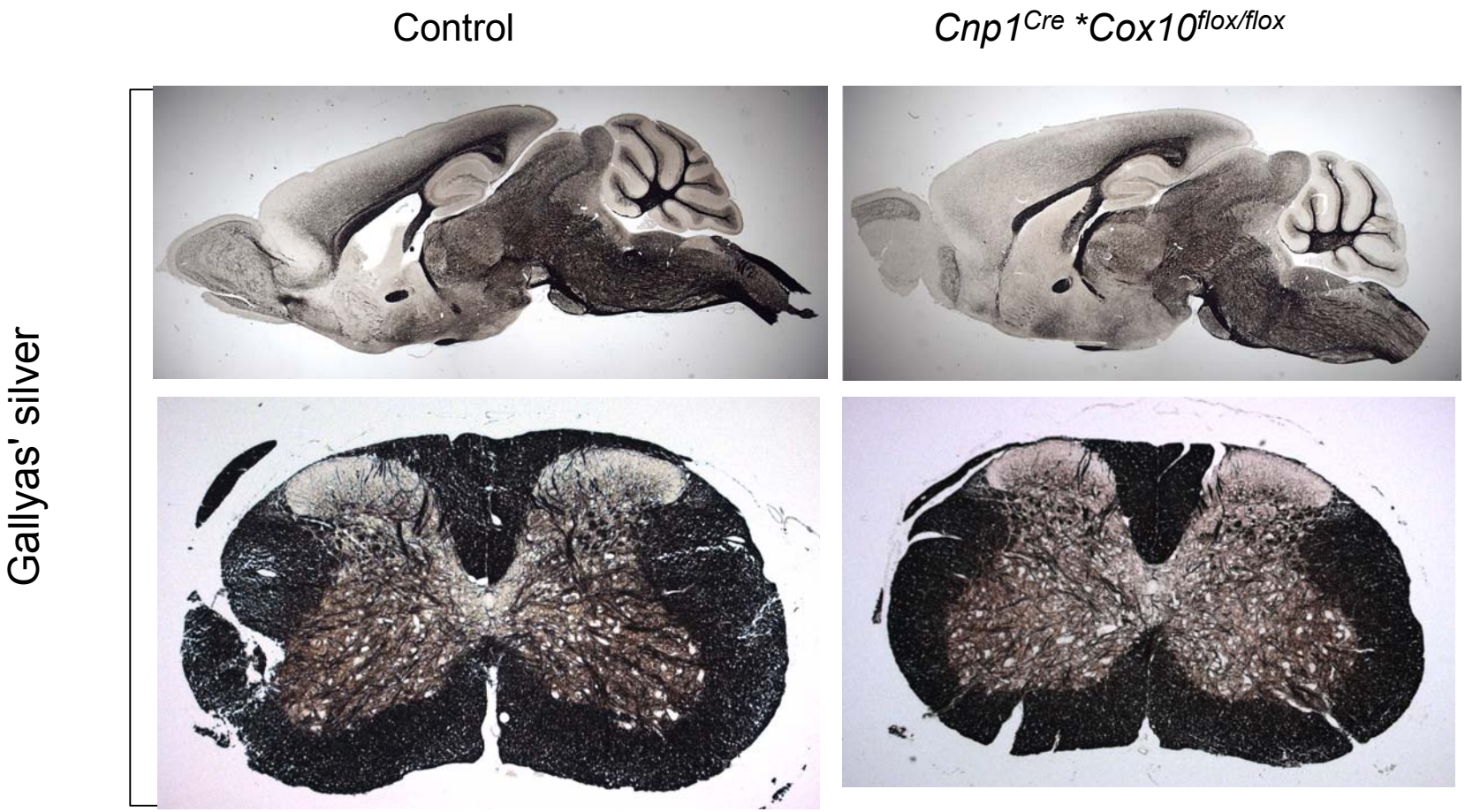

Suppl. Figure 4:

CNS myelination and white matter integrity
By Gallyas' silver impregnation of paraffin embedded CNS sections, no gross differences of myelination were detectable in brain (sagittal section, top) and spinal cord (bottom) at age 2 months.

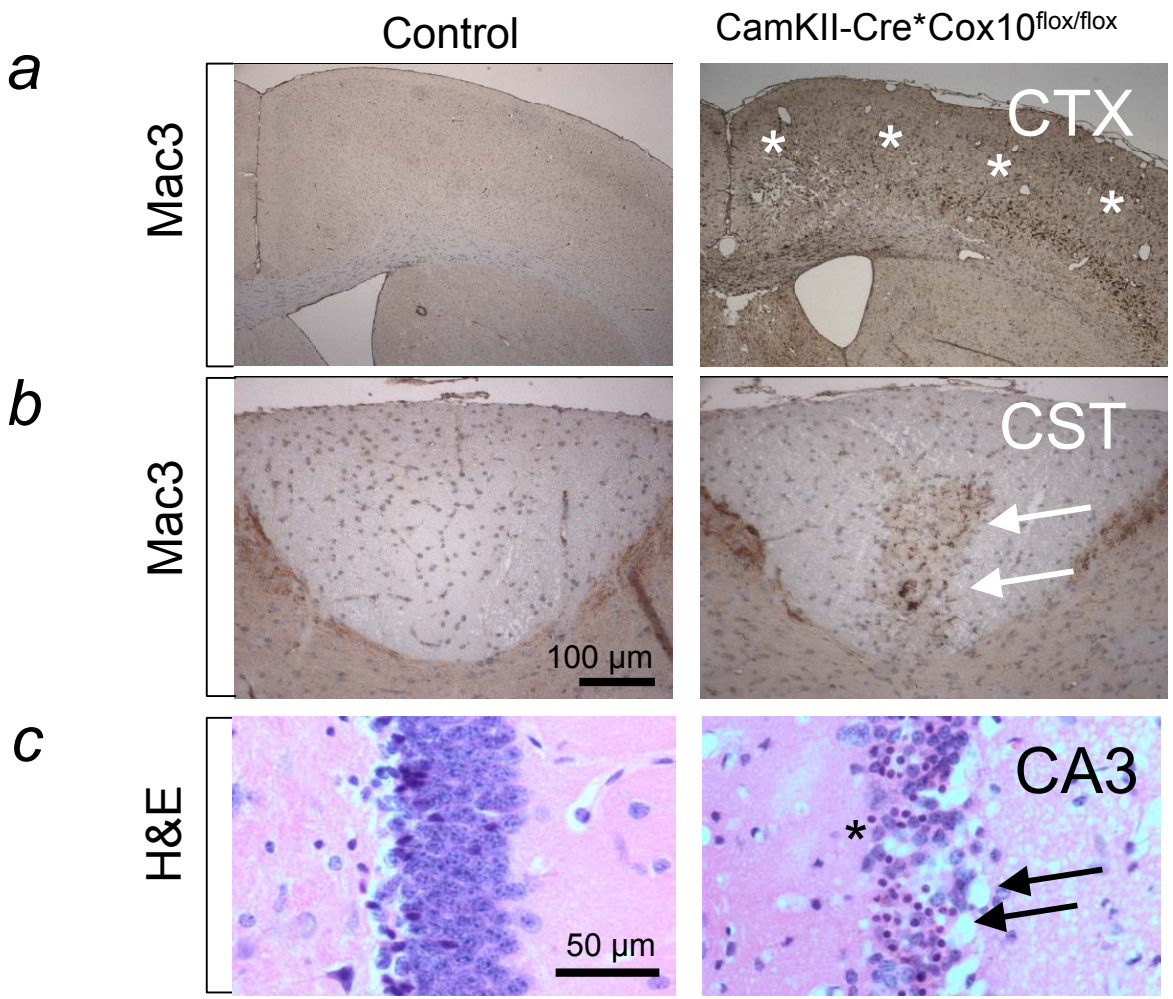

Suppl. Figure 5:

Neurodegeneration in CamKII-Cre*Cox10$^{flox/flox}$ mutants
(a, b) At age 4-5 months, Mac3 immunostaining (activated macrophages) revealed CNS areas with severe neurodegeneration in mutant mice (right), but not in controls (left), including neocortical layers (CTX) and the cortico-spinal tract (CST).
(c) Pyknotic nuclei (asterisk) and vacuolar lesions (arrows) in the hippocampal CA3 region, indicating widespread neuronal cell death in the CamKII-Cre expression domains.

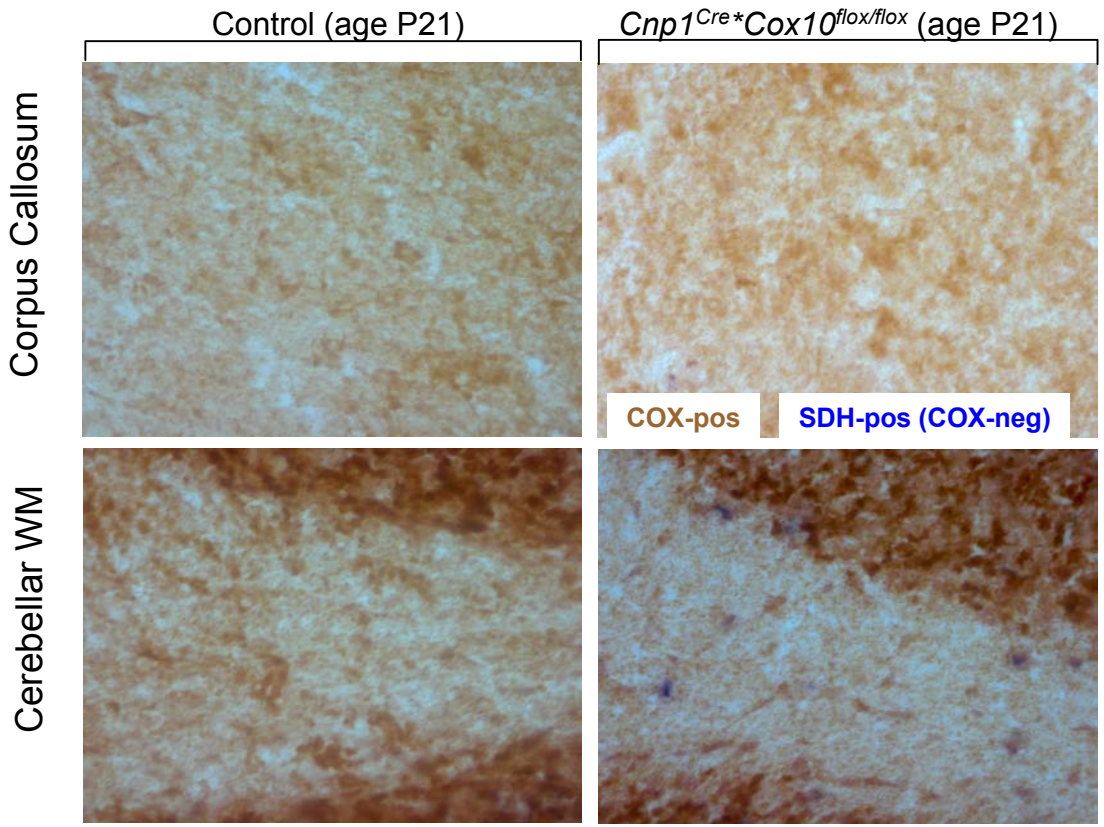

Suppl. Figure 6:

Intact mitochondria in oligodendrocytes from juvenile mice
By serial complex IV/complex II (SDH) histochemistry, white matter tracts of *Cnp1*^{Cre}**Cox10*$^{flox/flox}$ mutant mice aged P21 (top: corpus callosum; bottom: cerebellar white matter) reveal normal mitochondrial COX activity (brown precipitate). Blue cells (COX-negative) are not detectable, with few exceptions in the cerebellar white matter. Compare to Fig. 3g (age 9 mo).

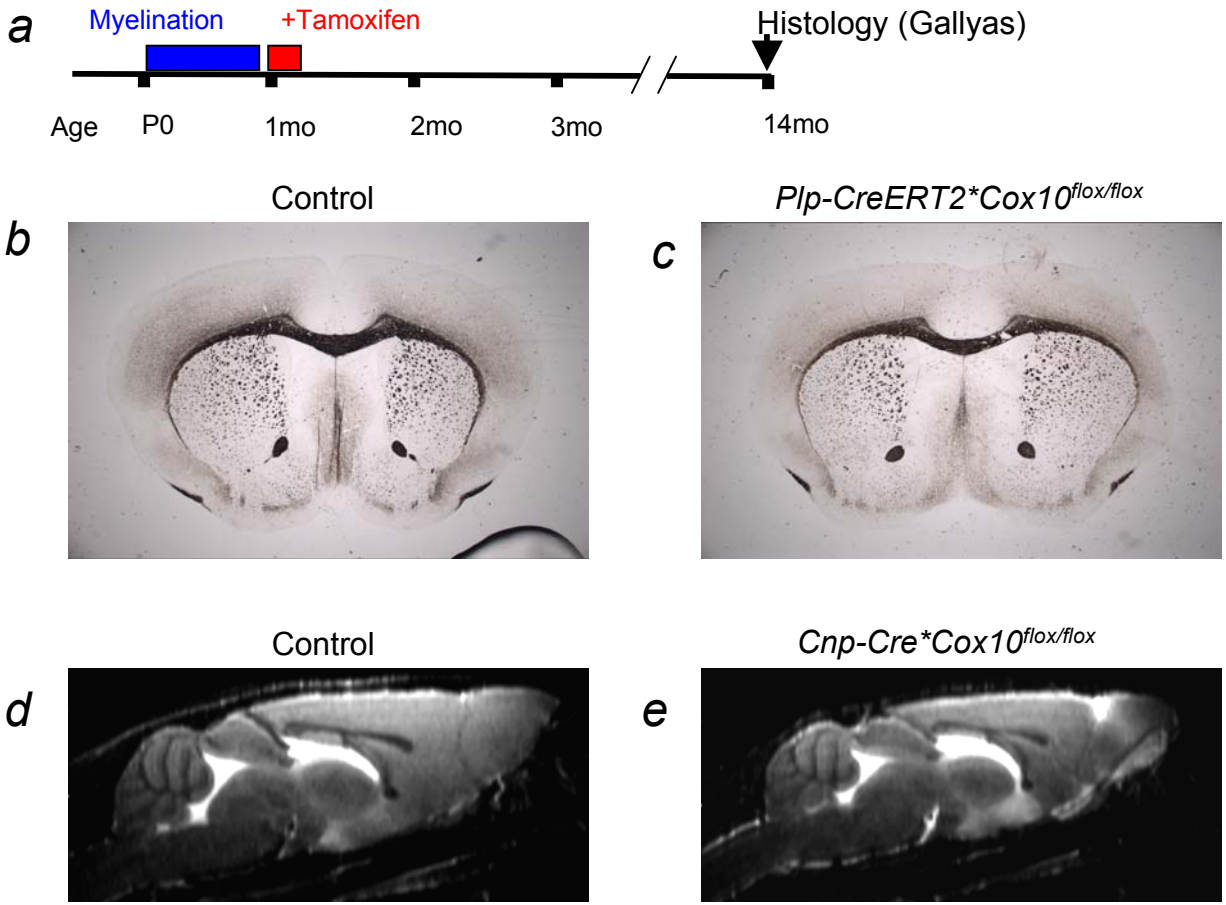

Suppl. Figure 7:

White matter integrity in *Cox10*$^{flox/flox}$ mutants.
(a) Time line of tamoxifen treatment of *Plp1-CreERT2*Cox10*$^{flox/flox}$ mice (following postnatal myelination) and analysis by histology more than a year later.
(b, c) Gallyas' silver impregnation of myelinated fiber tracts in tamoxifen-treated *Plp1-CreERT2*Cox10*$^{flox/flox}$ mutants and control mice at age 14 months (frontal section)
(d, e) MRI of *Cnp1*^{Cre}**Cox10*$^{flox/flox}$ mutants and control mice at age 6-7 months (sagittal image) show no signs of ventriclar enlargement (mutants 8.1 ± 1.1 mm^3, controls 8.4 ± 1.4 mm^3)

a $Cnp1^{Cre}*Cox10^{flox/flox}$

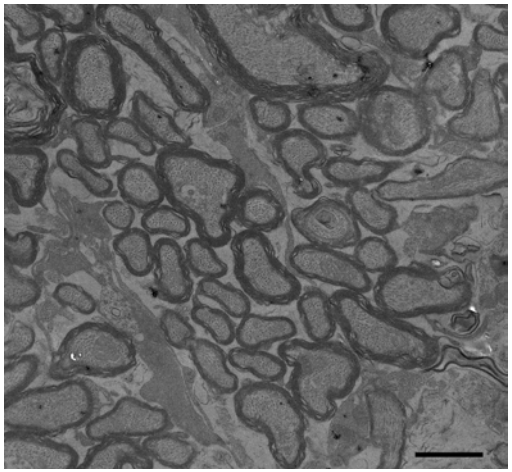

b Control

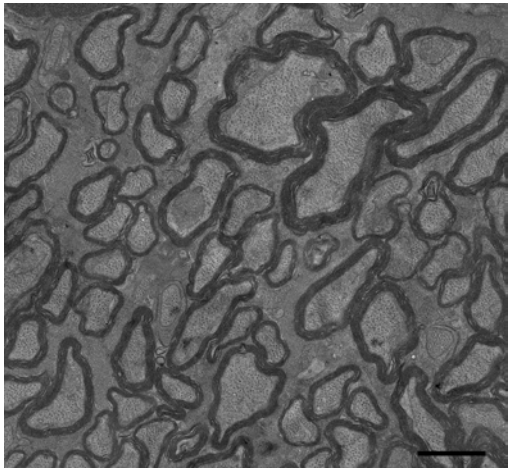

c

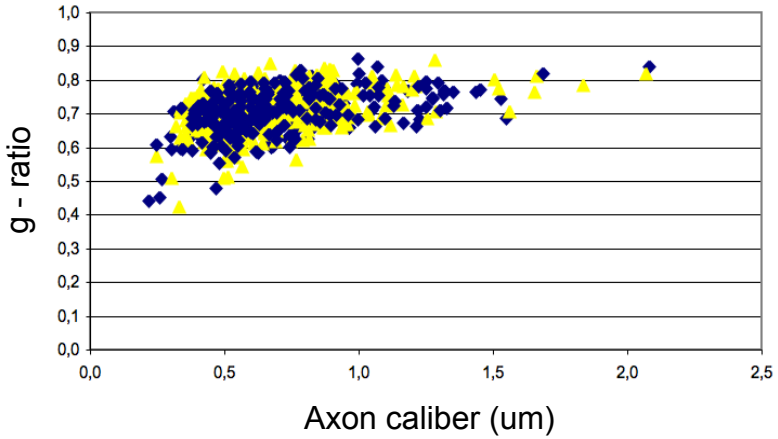

	g-ratio (± s.d.)
Mutant (yellow)	0.715 ±0.004
Control (blue)	0.705 ±0.003

Suppl. Figure 8:

Myelin sheath thickness in *$Cnp^{Cre}*Cox10^{flox/flox}$* mutants.
(a, b) Electron micrographs of the optic nerve in mutants and controls (age 9 months) used to determine g-ratios.
Scale bars, 1 µm.
(c) g-ratio analysis of adult optic nerve myelinated axons as a function of axon size fails to reveal dysmyelination.

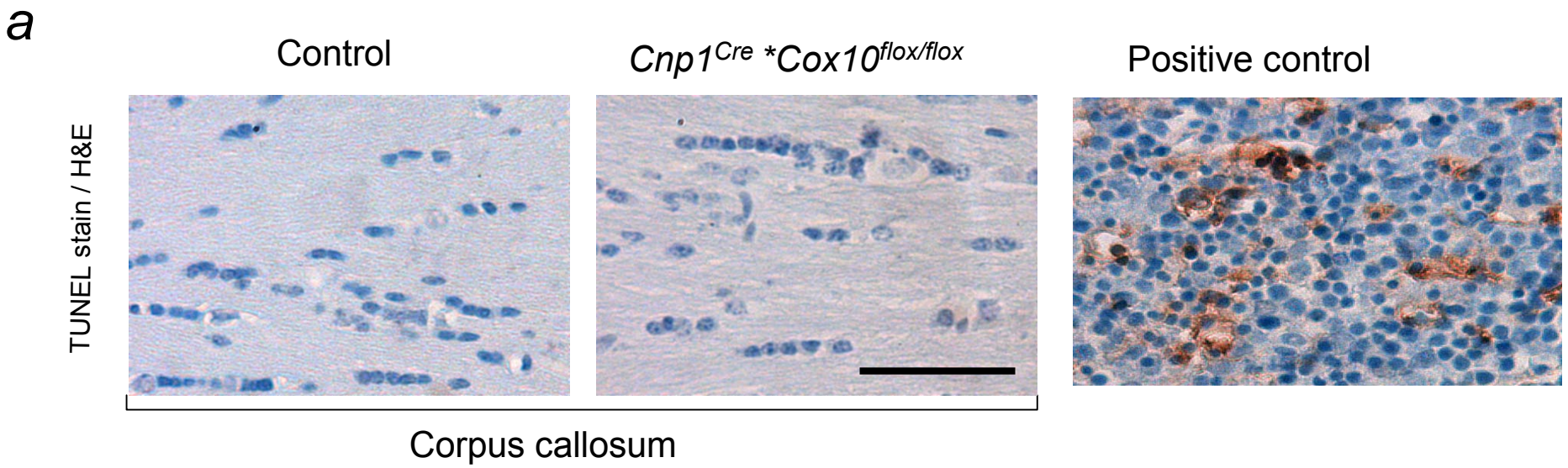

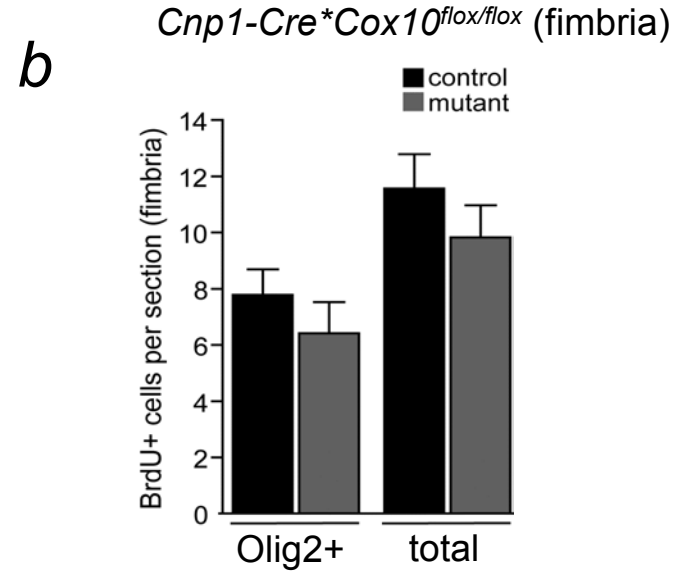

Suppl. Figure 9:

TUNEL assay and BrdU labelling of white matter tracts

(a) By TUNEL labeling of the corpus callosum (age 9 months), control brains (left) and *Cnp1*^{Cre}**Cox10*$^{flox/flox}$ mutant brains (middle) reveal no apoptotic oligodendrocytes, in contrast to a positive control (normal embryo, right). Scale bar, 100µm.

(b) Following daily administration of BrdU, the density of mitotic Olig2+ cells (left) in the fimbria of mutant mice and controls is the same. Similarly, there is no significant difference in the total number of BrdU positive cells (right). Numbers are ±s.e.m.

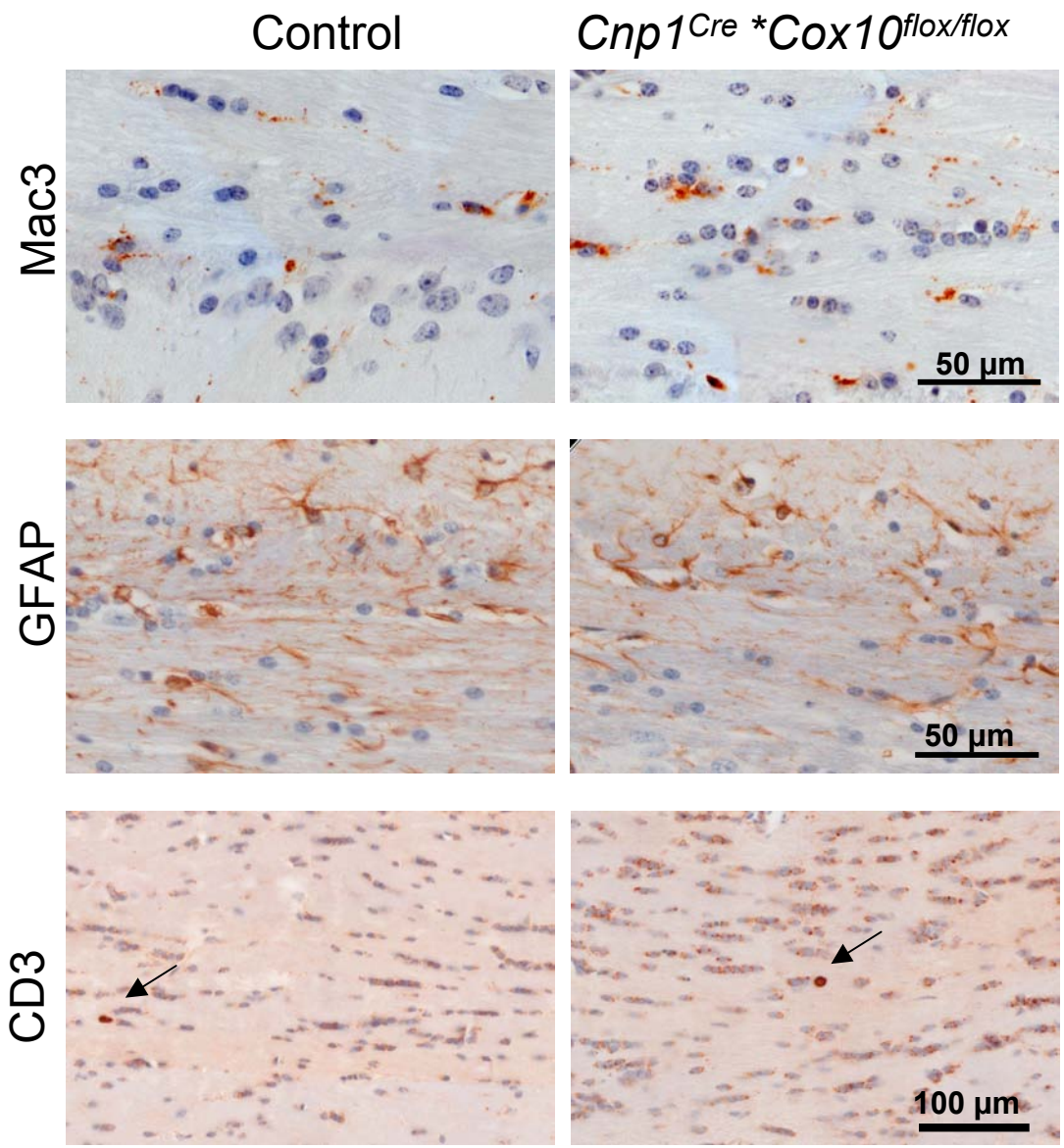

Suppl. Figure 10:

Absence of inflammatory signs of neurodegeneration

By immunostaining the corpus callosum of mutant mice (right) and controls (left) for Mac3 (activated microglia/macrophages, top), GFAP (astrogliosis, middle), and CD3 (invading T cells, arrow pointing to a single lymphocyte, bottom), the brains of *Cnp1*^{Cre}**Cox10*$^{flox/flox}$ mice exhibited no signs of neurodegeneration (age 9 months).

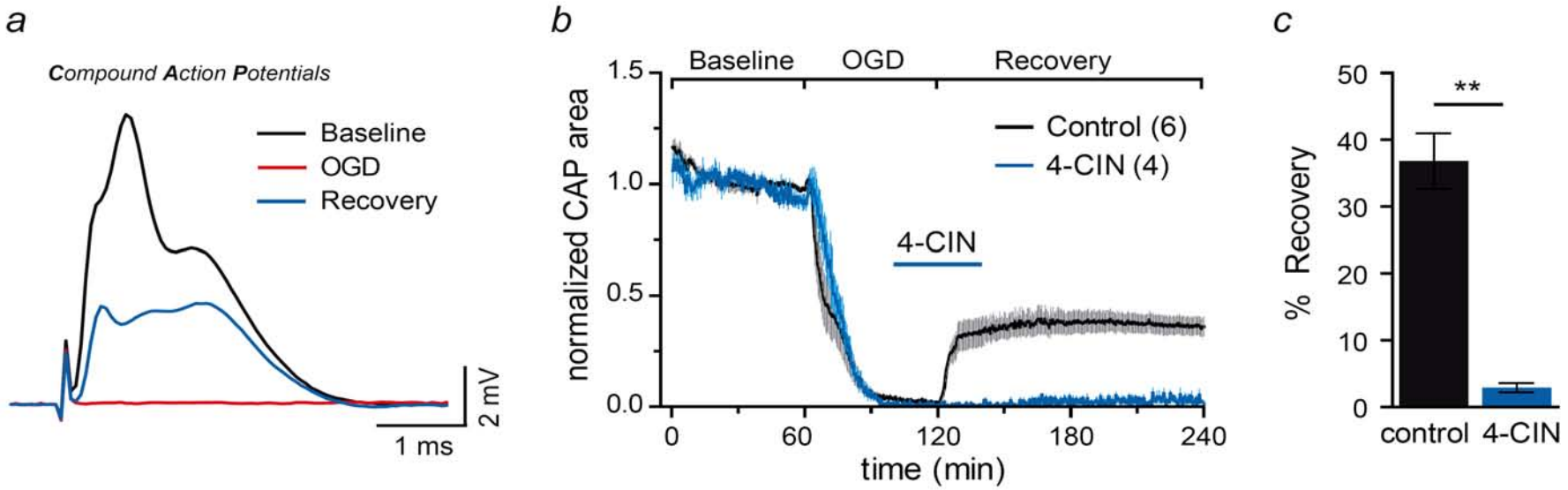

Suppl. Figure 11:

Functional recovery of energy-deprived myelinated optic nerve axons with glucose is perturbed by blocking MCT1 and MCT2.

(a) Myelinated optic nerves from adult wildtype mice, acutely dissected and repeatedly stimulated *ex vivo,* conduct impulses that are monitored as a compound action potential (CAP, Baseline). When exposed to oxygen-glucose deprivation (OGD, 60 min), the CAP gradually disappears due to complete energy failure and axonal conduction blocks (in red). However, axonal excitability can be partially recovered (in blue) by adding glucose to re-energize the axons (for details see Stys et al., 1990, PNAS 87, 4212-4216).
(b, c) This functional recovery of optic nerve axons after 60 min OGD is virtually impossible (with 10 mM glucose) when 200 µM α-cyano-4-hydroxycinnamic acid (4-CIN) is co-applied, a blocker of the monocarboxylate transporters MCT1 (in oligodendrocytes) and MCT2 (in axons), giving 36.8±4.2% vs. 2.9±0.7% CAP recovery with 10 mM glucose and 4-CIN co-application, respectively, *P*=0.0095, Mann Whitney *t* test. Thus, glucose must be converted to pyruvate or lactate and pass the glia and axonal monocarboxylate transporters in order to rapidly reenergize the axonal compartment.

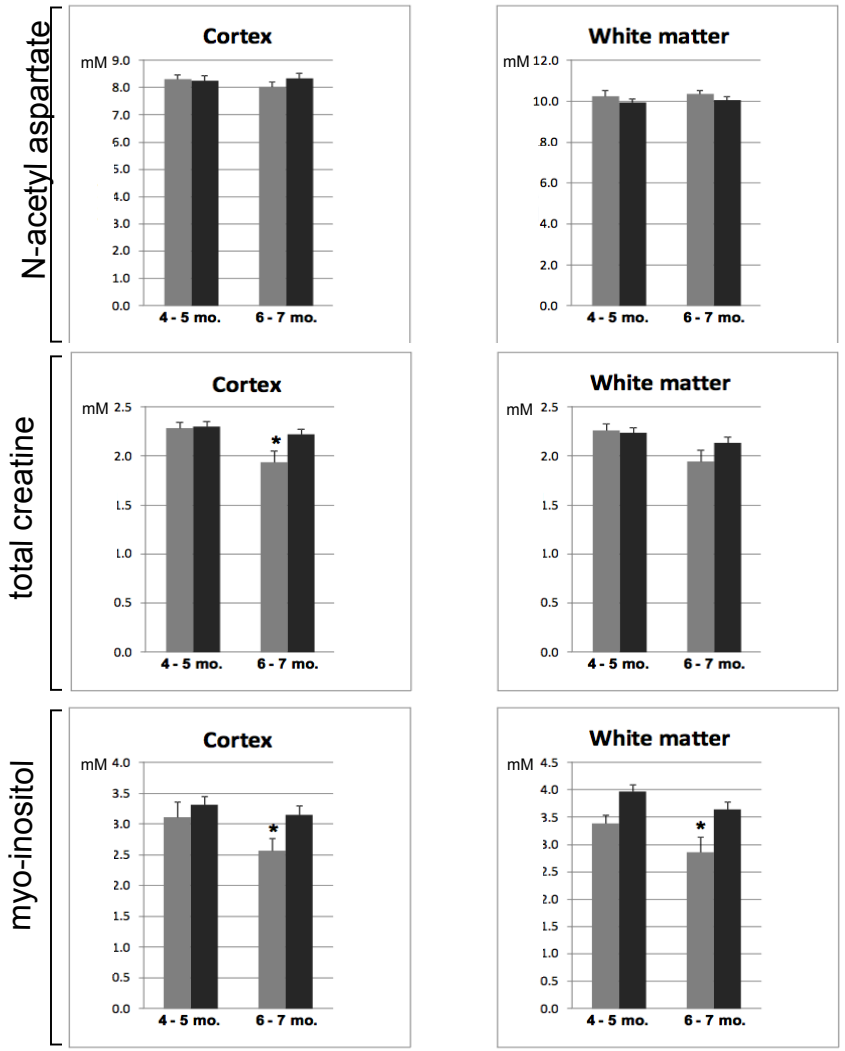

Suppl. Figure 12:

Localized proton MRS of metabolite concentrations in cortex and white matter

The level of NAA (top), creatine (middle), and myo-inositol (bottom) in cortex (left columns) and white matter (right columns) were determined at ages 4-5 months and 6-7 months (n=6-7 per genotype, mean±s.e.m., *p<0.05).